RSC Advances

ARTICLE

In-situ Mass Spectrometry Analysis of Chemical Vapour Deposition of TiO_2 Thin Films to Study Gas Phase Mechanisms

Ben J. Blackburn, Charalampos Drosos, Dean B. Brett, Michael A. Parkes, Claire J. Carmalt, Ivan. P. Parkin*

Received 00th January 20xx,
Accepted 00th January 20xx

DOI: 10.1039/x0xx00000x

www.rsc.org/

Deposition of TiO_2 thin films are studied using a newly developed in-situ mass spectrometry technique to observe gas phase reactions. Atmospheric pressure chemical vapour deposition (APCVD) reactions were carried out using titanium chloride and titanium tetraisopropoxide precursors, with ethyl acetate acting as an oxygen source in the case of the former, depositing on to float glass substrates at 300 and 600 ˚C.Using an atmospheric sampling mass spectrometer, the vapour phase was analysed during deposition and signals assigned to intermediate species that were measured during the formation of the thin films. The films deposited were characterised *via* scanning electron microscopy and thin film X-ray diffraction analysis.

Introduction

Chemical vapour deposition (CVD) is a technique used to produce thin films of a range of materials from carbon based materials, such as graphene[1] and diamond,[2] to biocompatible materials such as hydroxyapitite. Atmospheric pressure CVD (APCVD) is the most basic method of chemical vapour deposition, simply heating precursors to roughly half of its boiling point so that a vapour is evolved, then pushing the vapour to a heated reactor where it decomposes, depositing a film onto a substrate.[3] This method is commonly employed to deposit functional metal oxide thin films from simple molecular precursors, including TiO_2,[4–6] VO_2(M),[7–9] SnO_2, [10–12] Fe_2O_3, [13] WO_3, [14,15] ZnO,[16–18] α-Al_2O_3,[19,20] as well as many others.[21]

Despite widespread use in the deposition of metal oxide coatings, little is known about reactions that occur within the gas phase during the deposition of the thin film.[22] Part of the reason for this is the challenge in taking *in situ* measurement from the inside of a CVD reactor, as well as the potentially damaging nature of those vapours to analytical equipment.

Although uncommon, mass spectrometry studies of certain CVD reactions have been carried out in the past including deposition of cuprous films from copper(I) cyclopentadienyltriethylphosphine using a time-of-flight (TOF) spectrometer[23] and deposition of silicon carbide from a tetraethylsilane precursor using hot-wire CVD.[24] Rego, Petherbridge and Tsang *et al.* have completed mass spectroscopic studies on the CVD of diamond from methane, to measure the levels of CH_4, C_2H_6, C_2H_4 and C_2H_2 and CH_3 in the gas phase,[25] as well as the effect of N_2,[26] Cl_2,[27] and PMe_3[28] on the growth mechanics. In addition, analysis of titanium containing precursors have been carried out using mass spectrometry. Rahtu and Matero *et al.* used a similar system combined with a quartz crystal mass balance to analyse atomic layer deposition of titanium tetrachloride[29] and titanium(IV) isopropoxide[30] with deuterated water. These studies provided useful insight into the reaction of $TiCl_4$ with surface hydroxyl groups.

Herein we describe the use of a newly developed system to study the APCVD reactions for the deposition of TiO_2, using heated tubes to carry a sample of the reagent gas from the centre of the reactor chamber to a robust molecular beam mass spectrometer system (MBMS) capable of withstanding high temperature, corrosive species. The results provide an insight into the mechanisms occurring in the gas phase during the deposition of titanium dioxide thin films. TiO_2 thin films[31] and nanoparticles[32–34] are used in a range of technological applications, including self cleaning windows,[35–37] solar cells,[38] catalysis[39,40] and antimicrobial coatings.[37,41,42] In this work two of the most commonly used precursors for TiO_2 thin film deposition have been studied, namely titanium tetrachloride ($TiCl_4$) [43] and titanium tetraisopropoxide (TTIP).[44–46] With $TiCl_4$ an oxidising agent is required to produce TiO_2, such as ethyl aceatate,[46] whereas TTIP is frequently deposited alone due to the abundance of Ti-O linkages.

This work differs from the above examples in that the system developed was robust and versatile enough such that almost any CVD precursor could be studied *in-situ*, whilst still depositing thin films of a material. Also whilst the previous studies with titanium containing precursors focused on reactions with hydroxyl groups on the substrate surface, this study focuses on the gas-phase reactions, obtaining information on the formation of gaseous intermediates prior to deposition of the film onto the heated substrate.

Experimental

Department of Chemistry, University College London, 20 Gordon Street, London, WC1H 0AJ, UK
Electronic Supplementary Information (ESI) available: [details of any supplementary information available should be included here]. See DOI: 10.1039/x0xx00000x

Argon (Puresheild 99.998%) was obtained from BOC and used as supplied. Films of TiO_2 were deposited using a modified cold wall CVD reactor, onto 60 × 40 × 4 mm silicon coated float glass substrates, from Pilkington Glass Plc. The argon carrier gas was delivered into the system using stainless steel tubing. All of the tubing was heated to 150 ˚C using heater tape, monitored using by Pt-Rh thermocouples. The precursors ($TiCl_4$ + ethyl acetate and titanium isopropoxide) were introduced into the gas stream using a stainless steel bubbler, heated to 60 ˚C for $TiCl_4$ and 110 ˚C for titanium isopropoxide (TTIP) using a heater jacket. Hot argon or nitrogen was passed through the bubbler and the gas stream carried the precursor molecules to the reactor. When used, ethyl acetate was introduced through a second bubbler, heated to 35 °C (Figure 1). The amount of precursor was controlled using the flow rate of argon or nitrogen through the bubbler.

The reactor was heated to 300 or 600 ˚C. A stainless steel sampling tube, positioned above the substrate carried a sample of the reagent gas out of the reactor with the majority passing out of the rear of the reactor as exhaust. The sampling tube passed through a chamber bolted to the front of the mass spectrometer, allowing a small amount of the gaseous reactants to pass into the chamber through a hole in the tube. Both the chamber and the tube were heated to 200 ˚C, however due to the flow of hot air from the reactor, it was estimated that the temperature inside the tubing was higher. A small amount of the vapour entered the mass spectrometer through a metal cone with a fine aperture ¼ mm, fitted in the front end, which then formed a jet of molecules. The

remainder was carried away through the sampling tube or a secondary exhaust built into the front chamber.

The mass spectrometer used was a HPR-60 Molecular Beam Mass Spectrometer (MBMS) featuring an inlet approximately 0.25 mm in diameter leading into three consecutive vacuum chambers of increasingly low pressure (Figure 2). This design allowed mass spectrometry analysis to be performed by directly sampling from the reactor atmosphere. The inlet focused the gas entering the system into a beam that entered the ionisation chamber before ionisation *via* electron bombardment using a dual source low profile electron ionisation source, before separation of *m/z* species by quadrupole mass analyser. The quadrupole has a mass range of *m/z* 1 -1000. This system allows for the examination of extremely low concentrations of analyte compared to traditional spectrometers, enabling the analysis of transition metal species that would damage the detector in larger quantities. The MBMS instrument is ideal for high energy gas phase studies as upon entering the system the gaseous molecules undergo no further reaction, not coming into contact with each other or the walls of the detector. The detector was set to positive ion RGA mode for all measurements meaning that all species analysed are positively charged. The energy of the ionizing electrons was set to 70 eV for all experiments.

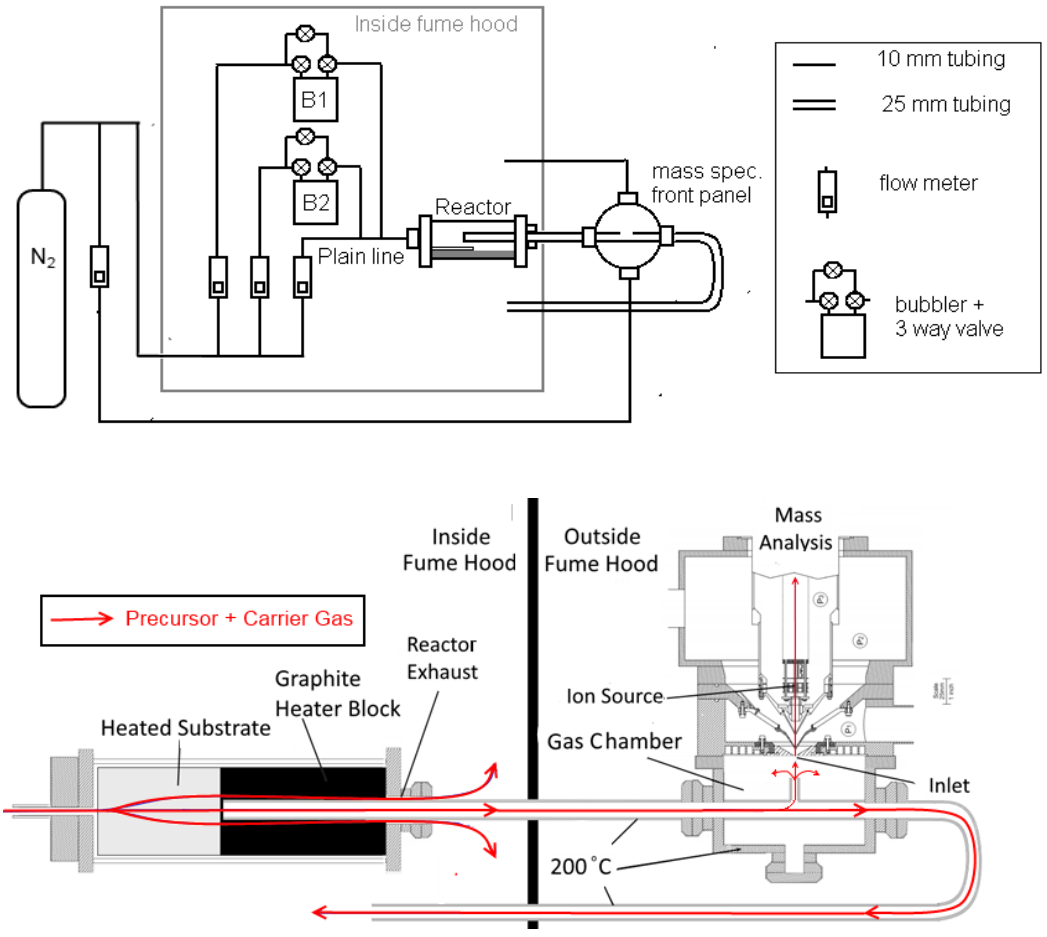

The mass spectrometer was set to scan continuously scan over a set *m/z* range of 50 – 500 Da (3 mins approx). After collecting a background as the sum of at least 10 scans, the precursor bubbler was opened in order to view the spectrum of the precursor only.

Table 1 Conditions for the four depositions with summary of the resulting mass spectra

No.	Precursor	Reactor Temp (˚C)	Bubbler Temp (˚C)	Bubbler Flow rate (L min^{-1})	Plain Line Flow Rate (L min^{-1})	EA bubbler Flow Rate (L min^{-1})	Observations
1	$TiCl_4$	300	60	0.4	2	0.4	Spectrum of $TiCl_4$ + ethyl acetate fully visible
2	$TiCl_4$	600	60	0.4	2	0.4	Spectrum of $TiCl_4$ + ethyl acetate fully visible. New peaks above molecular ion peak observed.
3	TTIP	300	110	0.2	6	-	Spectrum of TTIP fully visible
4	TTIP	600	110	0.2	6	-	Spectrum of TTIP heavily reduced. New peaks above molecular ion peak observed

In the case of the $TiCl_4$ depositions, the ethyl acetate oxidising agent bubbler was then opened, and the spectra of both reagents in the gas stream was observed. Each time either of the bubblers was turned on or the flow rates altered, the mass spectrometer was allowed to take 10 scans. This was chosen as it allows for enough scans to identify anomalous results, which can be the result of impurities or build-up of charge inside the mass spectrometer ion optics, whilst still preventing overexposure of the detector to the gas stream, which can lead to blockages and damage. In each case the spectrum of each deposition was generated by taking an average for each of sampled the *m/z* values for ten collected scans, then subtracting the background taken prior to the deposition.

Depositions with $TiCl_4$ were carried out with a flow rate through the bubbler of 0.4 L min^{-1} with a plain line flow rate of 2 L min^{-1}, whereas with TTIP the bubbler flow was set to 0.2 L min^{-1} and the plain line at 6 L min^{-1}. This was due to the TTIP forming particulates of TiO_2 that blocked the spectrometer inlet unless properly diluted with nitrogen.

Results and Discussion

Atmospheric pressure chemical vapour deposition (APCVD) was carried out using $TiCl_4$ and ethyl acetate or titanium isopropoxide (TTIP) at 300 ˚C and 600 ˚C with *in-situ* analysis of the reaction chamber using a molecular beam mass spectrometer. The films deposited at 600 ˚C for both precursors were thick and translucent, showing characteristic birefringence. The film deposited at 300 ˚C from $TiCl_4$ and ethyl acetate was a very thin, fine powder of TiO_2, not adherent and easily removed from the substrate.

Fig. 3 Mass spectrum of $TiCl_4$ as passed through a CVD reactor at 600 ˚C without ethyl acetate

The film deposited from TTIP at 300 ˚C was more adherent than that deposited from $TiCl_4$ at the same temperature, but failed the Scotch Tape test, and was fairly patchy and opaque. The resulting films were characterised using thin film X-ray diffraction analysis (XRD) and scanning electron microscopy (SEM).

Titanium tetrachloride + ethyl acetate: The EI mass spectrum obtained for $TiCl_4$ vapour alone at reactor temperatures of both 300 ˚C and 600 ˚C gave signals at *m/z* 189, 154, 118 and 83. The peak at *m/z* 189 represents the molecular ion $[TiCl_4]^{+\bullet}$, with the signals at *m/z* 154, 118 and 83 representing subsequent chlorine losses (-35 Da) resulting in the lower *m/z* value peaks (Figure 3). A weak signal at *m/z* 225 represents $TiCl_4$ having been further chlorinated by a chloride radical in the ionisation chamber. The formation of such ion species is possible in mass spectrometry when using hard ionisation sources such as electrospray ionisation.[47]

When the bubbler containing ethyl acetate was opened, new peaks were observed at *m/z* values in excess of the molecular ion $[TiCl_4]^{+\bullet}$, the highest of which was at *m/z* 314. This fits with two ethyl acetate molecules coordinating directly to the metal centre of the $TiCl_4$ resulting in the subsequent loss of chlorine. The *m/z* value of this signal suggests that the species has also undergone the loss a single methyl group from one of the ethyl acetate molecules, likely occurring at the ionisation source (Figure 4). This is confirmed by the isotope pattern of the peak which suggests the presence of only three chlorine atoms. The ethyl acetate/$TiCl_4$ coordinate species is likely the first step in the formation of the TiO_2 thin film.

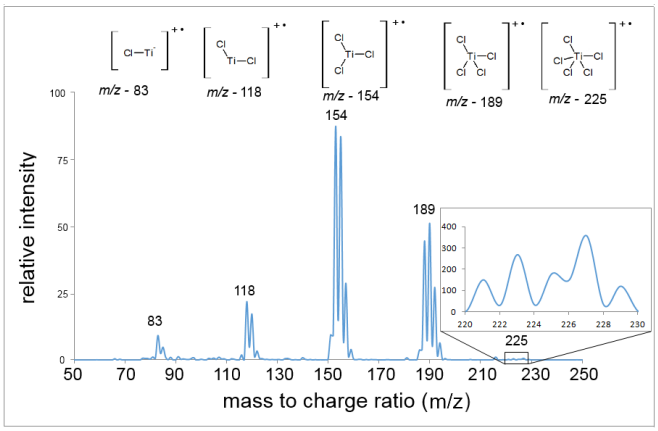

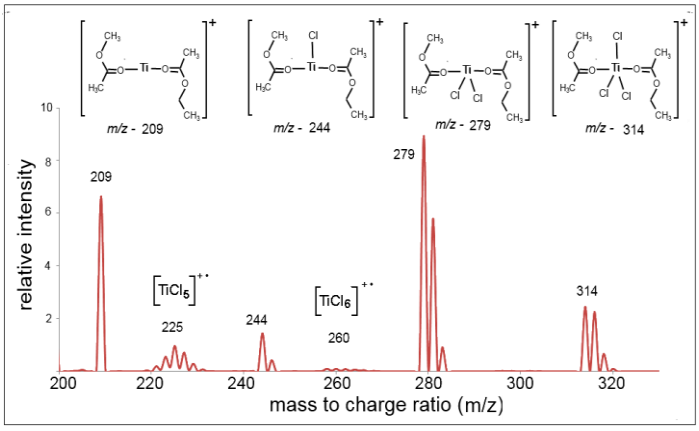

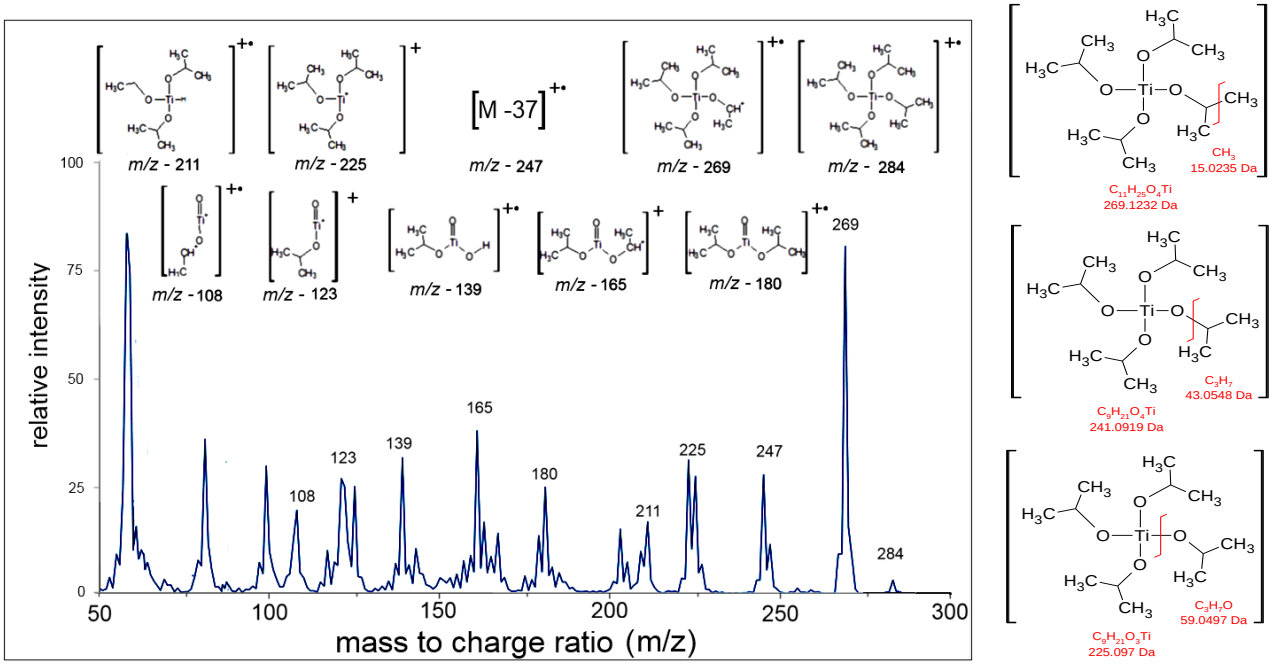

Fig. 5 Mass spectrum of gas within a CVD reactor during deposition with titanium tetraisopropoxide at 300 ˚C

Fig. 4 Mass spectrum of $TiCl_4$ as passed through a CVD reactor at 600 ˚C with ethyl acetate

The organic and chorine components of the unstable gaseous complex are likely removed upon contact with the heated substrate, leading to surface nucleation.

Subsequent peaks at *m/z* 279, 244 and 209 represent subsequent losses of further chlorine, most likely within the ionisation chamber of the mass spectrometer, after leaving the reaction. These peaks were only visible in the mass spectrum generated at 600 ˚C, implying that at the lower temperature of 300 ˚C the two reagents do not have enough energy to react in this way (ESI-1). At the lower temperature, no film was deposited, only a fine dust of TiO_2 particles, suggesting that this gas phase reaction is an intermediate in TiO_2 thin film formation. The removed chlorine ligands were not observed in either case as the m/z of a single chlorine atom would be 35 and 37, below the cut-off point of the scan.

Titanium Isopropoxide: Mass spectra were obtained from depositions using titanium isopropoxide alone at 300 ˚C and 600 ˚C, with strikingly different results. In both cases the abundance of alkoxide groups lead to far more complex spectra than the $TiCl_4$, which only involved loss of chlorine and methyl groups. The deposition at 300 ˚C gave a range of peaks, representing 15 major groups of *m/z* fragments, with proton losses leading to many more minor products. The heaviest ion (greatest *m/z* value) of these was the TTIP molecular ion, at *m/z* 284. Subsequent fragmentation is likely the result of the 'hard' nature of the electron ionisation used with the base peak present at *m/z* 269 representing homolytic cleavage of a carbon-carbon bond and the loss of a methyl group.

The molecular ion peak $[M]^{+\bullet}$ of TTIP was extremely weak, the most abundant ion corresponding to the loss of a single methyl group $[M-15]^{+\bullet}$ from one of the isopropoxide ligands. This is a phenomenon commonly observed in the ionisation chambers of EI mass spectrometers,[48] suggesting that the mass spectrum generated here is a very close approximation to putting TTIP through an EI instrument directly.

This mass spectrum is similar to one taken from an atomic layer deposition reactor used to deposit TiO_2 with titanium isopropoxide at 250 ˚C.[49] The major difference between the two spectra appears to be the emergence of a doublet signal at *m/z* 247 and 245, the structure of which could not be assigned as it does not correspond to the loss of a simple fragment. Fragmentation is complex although assignments have been made based on fragmentation occurring at the Ti-O bond, the O-C bond and the C-C bonds, resulting in the loss of a methyl (mass = 15 amu), propyl (mass = 43 amu) or isopropyl (mass = 59 amu) group respectively (Figure 6). It should be noted that only the fragmentations at the C-C bonds and Ti –O bonds occur in the first instance of fragmentation from the molecular ion, although fission of the C–O bond is observed in lower *m/z* fragmentations.

The deposition at 600 ˚C gave a very different pattern to that observed at 300 ˚C (Figure 7). In this case a new set of *m/z* peaks, many above the *m/z* value of the molecular ion were observed. The initial assumption when observing the repeating pattern of 60 amu decreases in the fragment masses was that the product was simply a polymer consisting of removed isopropoxide ligands potentially polypropylene glycol. It should be noted that the spectrum of the TTIP molecule observed at 300 ˚C is still visible but heavily reduced, suggesting that the majority of the molecular precursor is consumed by the reaction, converting into the oligomeric species or depositing onto the substrate. Furthermore the most heavily abundant peaks in the spectrum are the cluster of signals at *m/z* – 60, the top of which are cut off in figure 7. These relate to 2-propanol fragments, with

corresponding proton losses which would be expected as a dominant fragment for titanium isopropoxide.

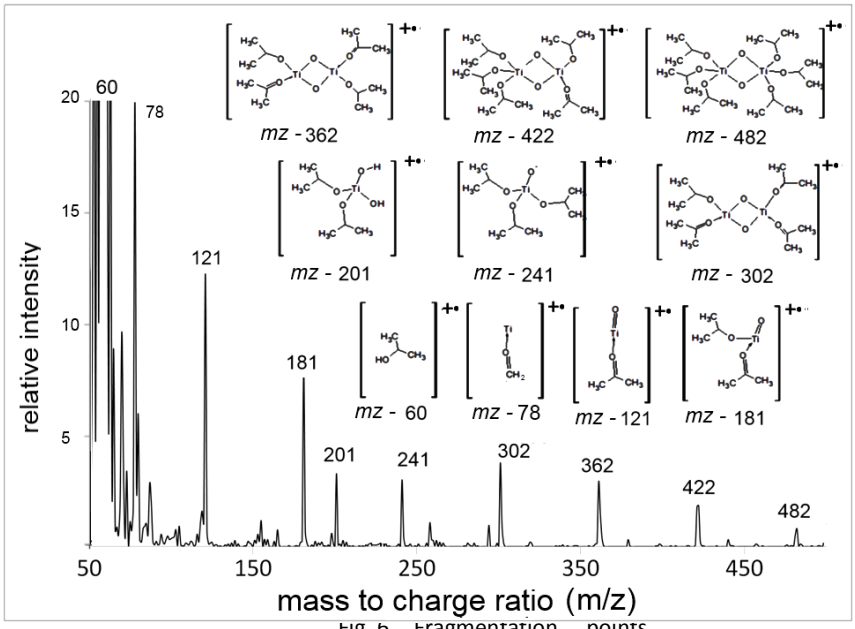

Fig. 7 Mass spectrum of gas wit with titanium tetra isopropoxide

Fig. 6 Fragmentation points on the TTIP parent ion.

ruled out that the ligand would coordinate to a proton later. The central carbon atom of the propane would be the most likely provider of a proton due to the tertiary nature of the carbon providing greater stability for the negative charge was well a being adjacent to the oxygen. The oxygen from one isopropoxide abstracts

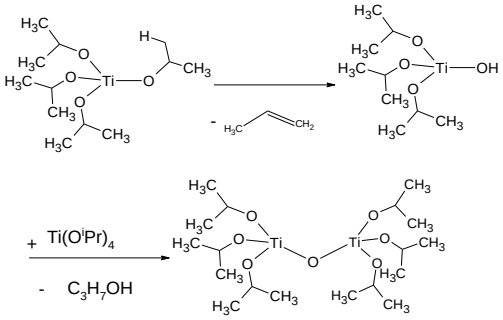

Fig. 8 Proposed formation of an oxo-bridge between two titanium isopropoxide molecules at high temperatures.[51]

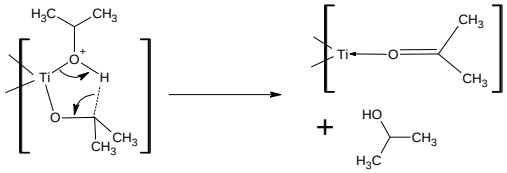

Fig. 9 Proposed mechanism for the loss of the elimination of an isopropanol molecule from TTIP and its dimer at high temperatures.

However the difference in *m/z* between the fragments would then be 58, as a proton would have to be lost from either end of the monomer.[50] The formation of an oxo-bridged dimer species in titanium isopropoxide has been proposed as a possible mechanism for the formation of nanoparticles via the solvothermal synthesis of TiO_2 from TTIP and benzylamine.[51] It is thought that the high temperature leads to the loss of the propyl group leaving an unstable $(O^iPr)_3TiOH$ (Figure 8). In this APCVD reaction it appears as though a dioxo bridge has formed between the two titanium centres. This would likely be a weak interaction with electron density shared over the two oxygen atoms forming a four membered ring.

The formation of the two oxo bridges without the loss of the isopropyl ligands would be highly disfavoured due to the two required Ti(V) species, therefore it is likely that the two bridging oxygen atoms are hydroxyl ligands, both of which could easily lose a proton in the mass spectrometer ionisation chamber. This would explain how such a species would be stable and would correspond to the small peak at *m/z* 484. If this is indeed the case, deprotonation of the bridging species could be a viable path for the loss of the isopropanol fragments.

Following the formation of the dimer species, fragments were lost of *m/z* - 60. As with the polymer this is not simply a case of heterolytic fission causing loss of the ligand, as would occur in an ionisation chamber, as the fragments would have an *m/z* of 59. The isopropoxide ligand group must be abstracting a proton as it leaves, forming isopropanol. The most likely pathway for the loss of isopropanol from the ligand is via the abstraction of a proton from another isopropyl ligand. This is corroborated by the presence of a large peak at *m/z* - 60 in the mass spectrum, however it cannot be the central proton from the adjacent ligand, resulting in the formation of an acetone group which remains coordinated to the metal centre (Figure 9). The broadened peak at around *m/z* 60 ligand is higher than the tallest precursor peak by a factor of 10:1 at 600 ˚C and 1:1 at 300 ˚C, which is expected for the higher energy system. This species is formed in the CVD reactor, as these peaks were not observed during the deposition at 300 ˚C. Further reactivity occurs with the loss of more isopropanol molecules in this way. Should the dimer species be forming inside the CVD reactor it is likely a precursor for the deposition of crystalline TiO_2 at higher temperatures. As with the $TiCl_4$ / ethy;l acetate deposition, the high temperature intermediate likely triggers thin film deposition.

X-ray Diffraction Analysis

In both cases the film deposited at 600 ˚C were the more crystalline, both giving XRD patterns for anatase TiO_2 (Figure 10). The more powdery films deposited from both precursors at 300 ˚C were found to be considerably less crystalline than those deposited at higher temperatures, giving only very weak, broadened peaks that also suggest a small amount of crystalline anatase TiO_2. In the case of the film deposited from titanium isopropoxide this is likely due to a lack of crystallinity in the film deposited, and for films deposited from $TiCl_4$ and ethyl acetate, is simply due to lack of product, the sparse and thin powdery product not being in high enough quantity to produce a strong pattern.

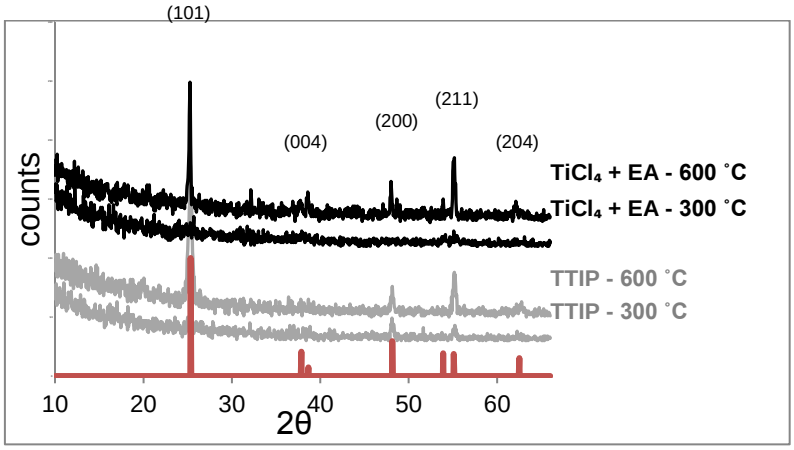

Fig. 10 X-ray diffraction pattern of the films deposited from (top to bottom) $TiCl_4$ and ethyl acetate at 600 and 300 ˚C and TTIP at 600 and 300 ˚C onto float glass using the APCVD / mass spectrometry apparatus, alongside an anatase TiO_2 standard.[54]

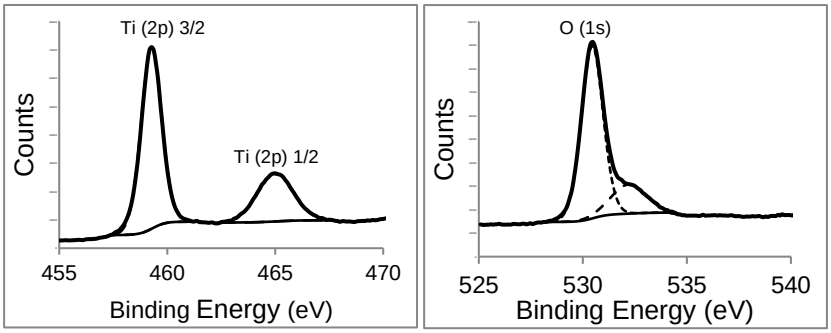

Fig. 11 Ti2p and O1s XPS spectra of the film deposited from $TiCl_4$ and ethyl acetate at 600 and 300 ˚C onto float glass using the APCVD / mass spectrometry apparatus.

Table 2. Atom % conc. of C, Ti and O in all four films deposited

	atom % conc			
	TTIP - 300 ˚C	**TTIP - 600 ˚C**	**TiCl4 + EA - 300 ˚C**	**TiCl4 + EA - 600 ˚C**
Carbon	57.68	42.77	74.97	29
Oxygen	35.81	45.38	22.54	53.37

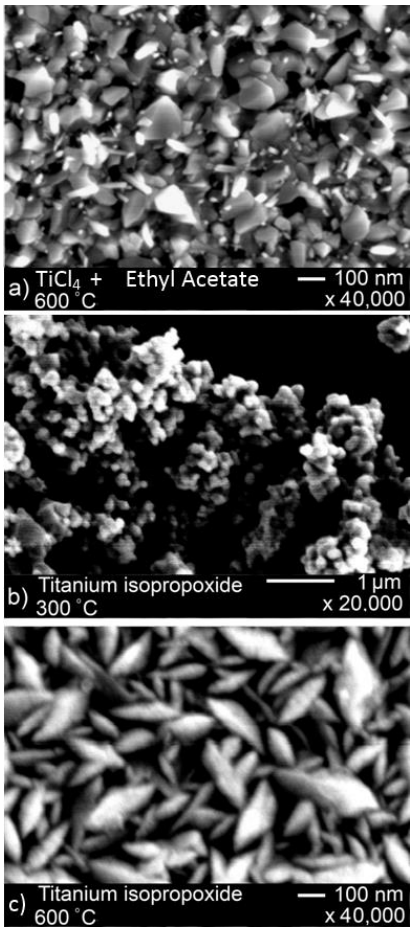

Fig. 12 SEM images of the film deposited from titanium chloride and ethyl acetate at 600 ˚C a) and titanium isopropoxide at 300 (b) and 600 ˚C (c) onto float glass using the APCVD / mass spectrometry apparatus

X-ray Photoelectron Spectroscopy

X-Ray photoelectron spectroscopy was conducted on a Thermo Scientific K-alpha spectrometer with monochromated Al Kα radiation, a dual beam charge compensation system and constant pass energy of 50 eV (spot size 400 µm). Survey scans were collected from 0–1200 eV. High-resolution peak data was collected for Ti (2p), O (1s) and C (1s). Data was fitted using CASA XPS software, with a doublet separation of 5.7eV for Ti (2p) signals.[55] In all four cases the XPS spectra of the films exhibit the peaks at 464.5 and 459.5 eV, commonly associated with titanium dioxide (Fig. 11), confirming the formation of some TiO_2 in all four depositions.[56] The atom% concentration of elements differs widely in each case (Table 2). The films deposited at 300 ˚C from TTIP and $TiCl_4$ have a carbon content of 57.68 and 74.94%, respectively, with the equivalent films deposited at 600 ˚C having considerably lower carbon contents of 42.77 and 29.00 atom%. Based on previous studies with these precursors it is likely the carbon has collected at the surface of the films. with the amount of carbon overestimated due to the surface sensitivity of XPS.[57, 58]

The titanium content of the films is below 20 atom% in each case, due to the titanium deficient nature of the anatase phase and the high carbon content. In the case of the TiO_2 film deposited from $TiCl_4$ and Ethyl acetate at 300 ˚C, the titanium content is only 2.49 atom%, which is in keeping with the observed lack of thin film formation on the substrate surface, and also explains the exceptionally high relative carbon content of the sample.

Scanning Electron Microscopy

SEM images were obtained for all four films. Imaging of the film deposited from $TiCl_4$ and ethyl acetate at 600 ˚C revealed a dense microstructure consisting of a mixture of thin plates roughly 200 nm in diameter and protruding rods of approximately 50 nm in diameter (Figure 12a). Imaging of the powdery substance deposited at 300 ˚C shows a substrate sparsely populated with roughly square

particulates of around 100 nm in diameter, with some areas more densely populated by particulates than others (ESI-2).

SEM micrographs of the titanium isopropoxide – deposited thin films also reveal a marked difference in morphology with deposition temperature. The film deposited at 600 ˚C consisted of flattened diamond shaped crystallites roughly 100 nm in width and between 200 and 300 nm in width, in a disordered arrangement with some perpendicular to the substrate an others lying flat. At 300 ˚C the film appears to display more pores, a disordered microstructure constructed of small grains of approximately 100 nm in diameter forming pseudo dendritic protrusions.

Conclusions

This study presents a new, versatile means of studying gas phase reactions in chemical vapour deposition, utilised in the study of two common means of depositing titanium dioxide, namely from titanium chloride with an ethyl acetate oxidising agent, and from neat titanium isopropoxide, both deposited via atmospheric pressure CVD. In both cases, the spectra obtained at the higher deposition temperatures suggests the formation of a high temperature mediated intermediate that could be partially responsible for the deposition of the resulting TiO_2 thins film.

The data from the SEM and XRD confirms the formation of TiO_2 thin films at elevated temperatures from titanium isopropoxide and $TiCl_4$ with an oxidising agent, as is well documented in the literature. [5,32,53,48] The pronounced difference in the mass spectra taken during depositions at 300 ˚C and 600 ˚C, as well as the resulting films, is strong evidence that the formation of the TiO_2 on the substrate surface strongly relates to the formation of the gas phase intermediate observed in the gas phase mass spectrum of the reactor atmosphere.

In the case of the $TiCl_4$ and ethyl acetate precursor mixture, it is evident that the intermediate $[TiCl_4(CH_3COOC_2H_5)_2]$ forms in the gas phase within the reactor vessel at high temperatures, followed by loss of ligands. As the measurement of this intermediate with mass spectrometry coincides with the successful deposition of a crystalline anatase TiO_2 thin film, it can be inferred that the reaction proceeds via this intermediate, before depositing onto the substrate, at which point the ligands are removed leaving only oxygen.

The case with titanium isopropoxide is less certain. The large number of signals, many of which are split by proton loss makes the mass spectra difficult to fully assign. However it is evident that the increase in temperature from 300 to 600 ˚C leads to a distinct change in the mass spectrum, with the majority of the peaks from the titanium isopropoxide molecular ion replaced by a new set of peaks, many of which are almost twice the *m/z* value of the molecular ion. The formation of titanium oxygen bonds within the gas phase before deposition would explain this phenomenon, with the resulting loss of whole isopropanol fragment via proton abstraction from other ligands evident in the considerable signal at *m/z* 60.

Acknowledgements

We would like to acknowledge the EPSRC and UCL Molecular Modelling and Materials Science EngDoc centre for funding these studentships (EP/G036675/1), furthermore BB would like to acknowledge Huntsman Pigments and Additives and CD and DB would like to acknowledge SAB Miller for providing additional funding, as well as Dr. Kirsti Karu for her invaluable contribution to the interpretation of the mass data.

1 Y. Zhang, L. Zhang and C. Zhou, *Acc. Chem. Res.*, 2013, **46**, 2329–2339.
2 J. G. Buijnsters, P. Shankar, W. Fleischer, W. J. P. Van Enckevort, J. J. Schermer and J. J. Ter Meulen, *Diam. Relat. Mater.*, 2002, **11**, 536–544.
3 K. Choy, *Prog. Mater. Sci.*, 2003, **48**, 57–170.
4 C. S. Chua, X. Fang, X. Chen, O. K. Tan, M. S. Tse, A. M. Soutar and X. Ding, *Chem. Vap. Depos.*, 2014, **20**, 44–50.
5 D. R. Patil, L. S. Patil, J. P. Bange and D. K. Gautam, *J. Optoelectron. Adv. Mater.*, 2008, **10**, 3251–3256.
6 D. Hocine, M. S. Belkaid, M. Pasquinelli, L. Escoubas, P. Torchio and a. Moreau, *Phys. Status Solidi*, 2015, **12**, 323–326.
7 D. Vernardou, D. Louloudakis, E. Spanakis, N. Katsarakis and E. Koudoumas, *Sol. Energy Mater. Sol. Cells*, 2014, **128**, 36–40.
8 P. Kiria, G. Hyett and R. Binionsa, *Adv. Mater. Lett.*, 2010, **1**, 86–105.
9 T. Manning, I. Parkin, C. Blackman and U. Qureshi, *J. Mater. Chem.*, 2005, **15**, 4560–4566.
10 D. Hatem and M. S. Belkaid, *Adv. Mater. Res.*, 2013, **685**, 166–173.
11 M. Maleki and S. M. Rozati, *Chem. Vap. Depos.*, 2014, **20**, 352–355.
12 C. Morales, H. Juarez, T. Diaz, Y. Matsumoto, E. Rosendo, G. Garcia, M. Rubin, F. Mora, M. Pacio and A. García, *Microelectronics J.*, 2008, **39**, 586–588.
13 C. C. Chai, J. Peng and B. P. Yan, *Advanced Nanomaterials and Nanotechnology: Proceedings of the 2nd International Conference on Advanced Nanomaterials and Nanotechnology*, Springer, 1995, 24.
14 S. Ashraf, R. Binions, C. S. Blackman and I. P. Parkin, *Polyhedron*, 2007, **26**, 1493–1498.
15 U. Riaz, *Thin Solid Films*, 1993, **235**, 15–16.
16 M. Pacio, H. Juárez, G. Escalante, G. García, T. Díaz and E. Rosendo, *Mater. Sci. Eng. B*, 2010, **174**, 38–41.
17 Y. Z. Yoo, S. H. Kim, G. S. Yoon, E. H. Choi, J. W. Park, J. H. Park, B. G. Kim, S. C. Jung and B. M. Park, *Appl. Phys. Lett.*, 2012, **100**, 1–4.
18 M. Maleki and S. M. Rozati, *Acta Phys. Pol. A*, 2015, **128**, 367–373.
19 S. Ruppi, *Int. J. Refract. Met. Hard Mater.*, 2005, **23**, 306–316.
20 S. Blittersdorf, N. Bahlawane, K. Kohse-Hoinghaus, B. Atakan and J. Muller, *Chem. Vap. Depos.*, 2003, **9**, 194–198.
21 C. E. Morosanu and G. Siddall, *Thin Films by Chemical Vapour Deposition, Volume 7, 1st Edition*, Elsevier, 2013**, 138–140.**
22 A. C. Jones and M. L. Hitchman, *Chem. Vap. Depos. Precursors, Process. Appl.*, 2009, 1–36.
23 A. E. Turgambaeva, N. Prud'homme, V. V. Krisyuk and C. Vahlas, *Chem. Vap. Depos.*, 2012, 18, 209–214.

24 X. M. Li, B. D. Eustergerling and Y. J. Shi, *Int. J. Mass Spectrom.*, 2007, **263**, 233–242.

25 C. A. Rego, P. W. May, C. R. Henderson, M. N. R. Ashfold, K. N. Rosser and N. M. Everitt, *Diam. Relat. Mater.*, 1995, 4, 770–774.

26 R. S. Tsang, C. A. Rego, P. W. May, M. N. R. Ashfold and K. N. Rosser, *Diam. Relat. Mater.*, 1997, 6, 247–254.

27 J. R. Petherbridge, P. W. May, S. R. J. Pearce, K. N. Rosser and M. N. R. Ashfold, *J. Appl. Phys.*, 2001, **89**, 1484–1492.

28 R. S. Tsang, P. W. May, M. N. R. Ashfold and K. N. Rosser, *Diam. Relat. Mater.*, 1998, **7**, 1651–1656.

29 R. Matero, A. Rahtu and M. Ritala, *Chem. Mater*, 2001, **13**, 4506–4511.

30 A. Rahtu and M. Ritala, in *CVD XV, proceedings of the fifteenth International Symposium on Chemical Vapor Deposition*, 2000, pp. 105–110.

31 T. Kemmitt, N. Al-Salim, M. Waterland, V. Kennedy and A. Markwitz, *Curr. Appl. Phys.*, 2004, **4**, 189–192.

32 K. Kaviyarasu, D. Premanand, J. Kennedy and E. Manikandan, *Int. J. Nanosci.*, 2013, **12**, 1350033.

33 F. Fang, J. Kennedy, E. Manikandan, J. Futter and A. Markwitz, *Chem. Phys. Lett.*, 2012, **521**, 86–90.

34 B. Sathyaseelan, E. Manikandan, V. Lakshmanan, I. Baskaran, K. Sivakumar, R. Ladchumananandasivam, J. Kennedy and M. Maaza, *J. Alloys Compd.*, 2016, **671**, 486–492.

35 C. Drosos and D. Vernardou, *Sol. Energy Mater. Sol. Cells*, 2015, **140**, 1–8.

36 A. V Emeline, A. V Rudakova, M. Sakai, T. Murakami and A. Fujishima, *J. Phys. Chem. C*, 2013, **117**, 12086–12092.

37 P. Marchand, I. A Hassan, I. P. Parkin and C. J. Carmalt, *Dalton Trans.*, 2013, **42**, 9406–22.

38 H. Chang and Y. L. Chen, *Jpn. J. Appl. Phys.*, 2010, **49**, 06GG04.

39 A. Mills, N. Elliott, I. P. Parkin, S. A. O'Neill and R. J. Clark, *J. Photochem. Photobiol. A Chem.*, 2002, **151**, 171–179.

40 A. L. Linsebigler, G. Lu and J. T. Yates, *Chem. Rev.*, 1995, **95**, 735–758.

41 V. Diesen, C. W. Dunnill, J. C. Bear, S. Firth, M. Jonsson and I. P. Parkin, *Chem. Vap. Depos.*, 2014, **20**, 91–97.

42 Y. Cai, M. Strømme, K. Welch, *PLoS One*, 8, 10, 1-8, 2013.

43 P. Evans, M. E. Pemble and D. W. Sheel, *Chem. Mater.*, 2006, **18**, 5750–5755.

44 C. S. Kim, K. Nakaso, B. Xia, K. Okuyama and M. Shimada, *Aerosol Sci. Technol.*, 2005, **39**, 104–112.

45 R. Binions and I. P. Parkin, in *Advances in Nanocomposites - Synthesis, Characterization and Industrial Applications*, ed. R. Boreddy, 2007.

46 A. J. Cross, C. W. Dunnill and I. P. Parkin, *Chem. Vap. Depos.*, 2012, **18**, 133–139.

47 S. Y. Park, M. S. Chun, J. S. Song and H. J. Kim, *Bull. Korean Chem. Soc.*, 2005, **26**, 575–578.

48 M. S. Lee, *Mass Spectrometry Handbook*, John Wiley & Sons, 2012.

49 A. Rahtu and M. Ritala, *Chem. Vap. Depos.*, 2002, **8**, 21.

50 G. Montaudo and M. S. Montaudo, *Z. Naturforsch*, 1980, **35a**, 1090–1097.

51 M. Niederberger and N. Pinna, *Metal Oxide Nanoparticles in Organic Solvents: Synthesis, Formation*, Springer Science & Business Media, 2009.

52 X. Chen and S. S. Mao, *Chem. Rev*, 2007, **107**, 2891–959.

53 S. A. O'Neill, R. J. H. Clark, I. P. Parkin, N. Elliott and A. Mills, *Chem. Mater.*, 2003, **15**, 46–50.

54 C. J. Howard, T. M. Sabine and F. Dickson, *Acta Crystallogr. Sect. B*, 1991, 47, 462–468.

55 NIST X-ray Photoelectron Spectroscopy (XPS) Database, Version 3.5 http://srdata.nist.gov/xps/ (accessed Nov 15, 2016).

56 U. Diebold and T. E. Madey, Surf. Sci. Spectra, 1996, **4**, 227.

57 S. Mathur, P. Kuhn, Surf. Coat. Tech., 2006, **201**, 807–814.

58 R. Gerbasi, A. Gregori, S. Cattarin, G.A. Ritazzi, Thin Solid Films, 2000, **371(1-2)**, 126-131.